

Conference paper

Zahra Ahali Abadeh, Giovanna Saviano, Paolo Ballirano and
M. Gabriella Santonicola*

Curcumin-loaded zeolite as anticancer drug carrier: effect of curcumin adsorption on zeolite structure

<https://doi.org/10.1515/pac-2018-1213>

Abstract: In this work we used a combination of different techniques to investigate the adsorption properties of curcumin by zeolite type A for potential use as an anticancer drug carrier. Curcumin is a natural water-insoluble drug that has attracted great attention in recent years due to its potential anticancer effect in suppressing many types of cancers, while showing a synergistic antitumor effect with other anticancer agents. However, curcumin is poorly soluble in aqueous solutions leading to the application of high drug dosage in oral formulations. Zeolites, inorganic crystalline aluminosilicates with porous structure on the nano- and micro-scale and high internal surface area, can be useful as pharmaceutical carrier systems to encapsulate drugs with intrinsic low aqueous solubility and improve their dissolution. Here, we explore the use of zeolite type A for encapsulation of curcumin, and we investigate its surface properties and morphology, before and after loading of the anticancer agent, using scanning electron microscopy (SEM), powder X-ray diffraction (XRD), differential scanning calorimetry (DSC), and UV-vis spectroscopy. Results are used to assess the loading efficiency of zeolite type A towards curcumin and its structural stability after loading.

Keywords: anticancer agent; curcumin; drug delivery; Eurasia 2018; zeolite type A.

Introduction

The interaction of pharmaceutical molecules with inorganic materials has been receiving considerable attention in recent years due to the increasing applications of such materials in drug delivery, particularly for targeted treatments of cancer [1, 2]. In cancer therapy, the safe and efficient delivery of chemotherapeutic drugs with low permeability and poor solubility in aqueous media is still a challenging task, which can be overcome through the use of drug-specific delivery systems. According to the World Health Organization (WHO), 8.2 million deaths in 2012 were linked to cancer, which is well-known as one of the diseases with highest mortality worldwide [3].


Conventional cancer treatment with chemotherapy has shown several limitations over the years, including insufficient drug concentrations, high cytotoxicity, and problems of multidrug resistance, namely the

Article note: A collection of invited papers based on presentations at the 15th Eurasia Conference on Chemical Sciences (EuAsC2S-15) held at Sapienza University of Rome, Italy, 5–8 September 2018.

***Corresponding author: M. Gabriella Santonicola**, Department of Chemical Materials and Environmental Engineering, Sapienza University of Rome, Via del Castro Laurenziano 7, 00161 Rome, Italy, e-mail: mariagabriella.santonicola@uniroma1.it.
<https://orcid.org/0000-0002-2736-8580>

Zahra Ahali Abadeh and Giovanna Saviano: Department of Chemical Materials and Environmental Engineering, Sapienza University of Rome, Via del Castro Laurenziano 7, 00161 Rome, Italy

Paolo Ballirano: Department of Earth Sciences, Sapienza University of Rome, P. le Aldo Moro 5, 00185 Rome, Italy

 © 2019 IUPAC & De Gruyter. This work is licensed under a Creative Commons Attribution-NonCommercial-NoDerivatives 4.0 International License. For more information, please visit: <http://creativecommons.org/licenses/by-nc-nd/4.0/>

Brought to you by | Università degli Studi di Roma La Sapienza
Authenticated | mariagabriella.santonicola@uniroma1.it author's copy
Download Date | 3/5/20 3:42 PM

ability of cancer cells to become simultaneously resistant to different drugs. Drug delivery systems have shown a higher efficiency in comparison with traditional drug treatments, but some challenges and limitation still remain. In order to overcome these problems, the development of novel drug delivery systems, such as those based on inorganic molecular carriers, would be highly beneficial. Among all the available inorganic drug carriers, numerous studies have investigated zeolite structures due to their unique properties, such as high adsorption capacity and specific surface area, water solubility, as well as good biocompatibility and stability in biological environments [4–6].

Zeolites are inorganic crystalline aluminosilicates with a porous structure on the micro- and nano-scale and high internal surface area, and they are well known as adsorbents, molecular sieves and ion exchange materials in many applications [7, 8]. In the medical and pharmaceutical fields, zeolites have recently emerged as promising materials due to their bioactive properties and good stability in biological environments [9, 10]. Many zeolites occur in nature as aluminosilicate minerals and more than 200 synthetic zeolites can be prepared in the laboratory [11]. Each zeolite framework has a unique structure, which is generally made of silicon, aluminum and oxygen atoms. The building blocks are arranged in a periodic way by connections among $[\text{SiO}_4]^{4-}$ and $[\text{AlO}_4]^{5-}$ units to form channels and cages, which endow the material with its characteristic microporous structure [12, 13]. The pores (α cage) of the zeolites are open, leading to the diffusion of molecules from the exterior to the interior of the zeolite particles. The structure of zeolite A (Linde type A) is characterized by small pores, as shown in Fig. 1, with each pore defined by an eight-member oxygen ring, which makes a larger cavity connecting eight sodalite cages on the edges of a cubic structure [14].

The unique combination of zeolite properties has resulted into different medical applications of zeolites, for example for the encapsulation and delivery of drugs with anticancer, antibiotics and antimicrobial properties [15]. In drug delivery, the zeolitic structures loaded with drugs could be administrated to a patient for health treatments, such as cancer therapy, without loss of the individual pharmacological effect of the products. In addition, zeolites can bind and encapsulate drugs with low aqueous solubility, thus increasing significantly their bioavailability in the physiological environment [16]. Regarding potential toxicity, it has been demonstrated that zeolite toxicity strongly depends on the size, shape and composition of the particles. Micro-sized zeolites characterized by FAU, LTA and LTL structures exhibit low levels of cytotoxicity even at high concentrations in cell culture medium. On the other hand, nano-sized zeolites show different

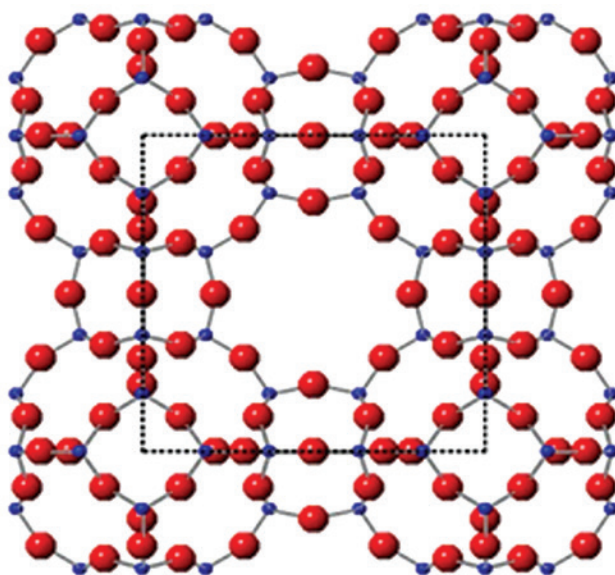


Fig. 1: Zeolite Linde type A (LTA) framework with the α cage as the unit cell in the middle (black square). Red: oxygen atoms; blue: Si/Al atoms [14].

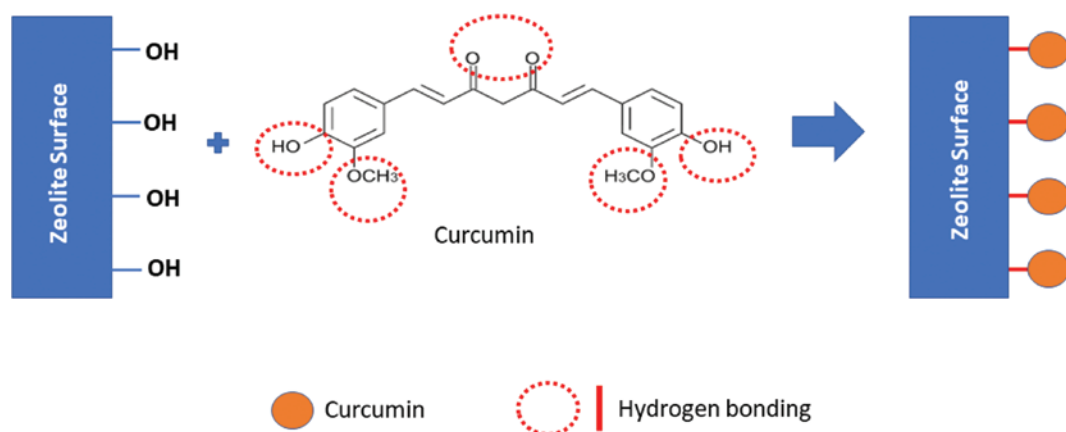


Fig. 2: Schematic of curcumin adsorption on zeolite surface.

cytotoxicities, and both alumina component and crystal shape have significant influence on their toxicity [17]. For example, pure silica nanozeolite with spherical morphology is nontoxic, but alumina-containing nanozeolites ZSM-5, LTL and LTA are toxic. This has been linked to the presence of surface acidic sites, which can catalyze chemical reactions of cell membranes and induce the necrosis of cells. In addition, surface charge plays an important role on nanoparticle toxicity: positive-charged surfaces are more toxic than negative-charged ones due to the strong affinity of cationic surface to negatively charged cell membrane [18].

Curcumin, the active ingredient of turmeric (*Curcuma longa*) plant, is a water-insoluble natural compound that has attracted great attention in recent years in biomedical science. Curcumin is a low-molecular-weight phenolic compound with a wide range of pharmacological actions and biological activities, including anti-cancer [19], anti-microbial, anti-inflammatory, and with low or no intrinsic toxicity for promising clinical applications [20, 21]. However, the limited solubility and rapid elimination of curcumin lead to poor bioavailability after oral usage or topical administration [22, 23]. As a consequence, curcumin needs to be applied in very high dosage in oral formulations. The use of a zeolite carrier for curcumin has the potential to render the drug dispersible and increase its bioavailability.

In our work, we analyse the ability of synthetic zeolite 5A, a Ca^{2+} exchanged form of zeolite LTA (Fig. 1), to load the bioactive compound curcumin, which is well-known for its therapeutic effects. Zeolite 5A has an effective pore opening of about 5 Å and Ca^{2+} ion as a coordinating cation in its structure, leading to a more uniform and stable drug delivery system.

The aim of this research was to determine the ability of synthetic zeolites with type A structure for loading curcumin by diffusion in liquid phase and adsorption on the surface or in the voids of the zeolite porous framework (Fig. 2). The effect of the curcumin concentration on the zeolite loading capacity was studied. The structural properties and morphology of the zeolite carrier, before and after curcumin loading, were investigated using scanning electron microscopy (SEM), powder X-ray diffraction (XRD), and differential scanning calorimetry (DSC). The encapsulation and adsorption of curcumin on the zeolites surface were analyzed as a function of concentration using UV-vis spectroscopy.

Experimental section

Materials and sample preparation

Zeolite 5A, the calcium-exchanged form of zeolite Linde type A, was obtained in bead form from Zeochem AG (Switzerland). According to the manufacturer datasheet, this type of zeolite has a nominal pore diameter of

5 Å. The beads were converted to powder before use by grinding in a ceramic mortar. The final product was in powder form with particles below 100 µm in size. Curcumin from *Curcuma longa* (turmeric) (IUPAC name (E,E)-1,7-bis(4-Hydroxy-3-methoxyphenyl)-1,6-heptadiene-3,5-dione and common name diferuloylmethane) was purchased from Sigma-Aldrich (Schnellendorf, Germany) and used as received. To evaluate the curcumin loading capacity, the zeolite powders were first dehydrated in oven at 120 °C overnight to eliminate any water inside the pores that would interfere with the adsorption process, and then incubated with the curcumin solution for 48 h. For each experiment, 500 mg of zeolite 5A were added to a solution (20 mL) made by dissolving curcumin at different concentrations (0.0125, 0.025, 0.05 mol/L) in acetone. The mixtures were stirred at room temperature for 48 h. During this time the original white color of the zeolite powder changed to yellow, indicating that curcumin was incorporated with the zeolite structure. After curcumin loading, the mixtures were filtered and the yellow solid was dried in oven at 50 °C for 12 h to remove residual solvent.

Characterization methods

UV-visible spectroscopy

UV-vis measurements were performed using a Shimadzu UV-2700 spectrophotometer in the range 400–500 nm (curcumin absorption peak $\lambda_{\max} = 419$ nm). Curcumin solutions were diluted with pure acetone and measured in quartz cells with 1 cm path-length. The zeolite loading capacity was determined by comparing the concentration of curcumin in the original incubation solution with the concentration of the supernatant after sedimentation of the loaded zeolites. Curcumin concentration in the supernatant was quantified through a calibration curve obtained from solutions of known concentration. From the calibration curve, the molar extinction coefficient of curcumin in acetone was determined to be $78\,297\text{ M}^{-1}\text{ cm}^{-1}$ at 419 nm.

X-ray diffraction (XRD)

X-ray diffraction patterns for the empty and curcumin-loaded zeolites were obtained with a Bruker D8 ADVANCE diffractometer (Bruker-AXS, Karlsruhe, Germany). All samples were analyzed in powder form. Diffraction data were collected in the 2θ range from 5° to 140° with counting time of 2 s, corresponding to an acquisition time of ~3.5 h per pattern. Rietveld refinement analysis of the XRD data was carried out to characterize the crystalline phases in terms of composition and crystallite size.

Scanning electron microscopy (SEM)

SEM analysis was carried out to investigate the microstructure and morphology of the empty and curcumin-loaded zeolites. In addition, quantitative elemental composition maps of the samples were acquired with an energy-dispersive X-ray (EDX) spectrometer. A Zeiss Auriga 405 field-emission microscope (FE-SEM) (Carl Zeiss, Oberkochen, Germany) equipped with a Quantax EDX detector (Bruker Nano, NJ, USA) was used for the investigation. Zeolite 5A and curcumin-loaded zeolite samples were analyzed without further sample preparation. Each sample was fixed on steel stub using carbon tape. Samples were analyzed at low accelerating voltage (2 kV) and with different magnifications to achieve high-resolution visualization.

Fourier-transform IR spectroscopy

Characterization of the functional groups was carried out with a Spectrum One FTIR spectrometer (Perkin-Elmer, Waltham, MA, USA) equipped with an attenuated total reflectance (ATR) element (ZnSe crystal).

Samples were analyzed at room temperature in the wavenumber range 4000–650 cm^{-1} by averaging 40 scans at a resolution of 4 cm^{-1} . All samples spectra were corrected against the background spectrum of air taken at the same instrumental conditions. FTIR spectra were processed using the Perkin-Elmer Spectrum software.

Differential scanning calorimetry (DSC)

The thermal properties of the zeolite samples were studied using a Perkin-Elmer Pyris 1 DSC instrument (Perkin-Elmer, Waltham, MA, USA). Samples (~5 mg) were sealed in aluminum pans and measured in the temperature range from 25 °C to 300 °C with a heating rate of 10 °C/min under nitrogen flow. Several samples (between three and four) were analyzed for each type of empty and curcumin-loaded zeolites to ensure reproducibility of results. An empty aluminum pan was used as the reference cell. Data were corrected by subtracting a baseline measured with an empty pan at the same conditions and were normalized by the sample weight. The Perkin-Elmer Thermal Analysis Software provided with the instrument was used for the peak analysis.

Results and discussion

In the present study, curcumin, a natural drug known for its anticancer properties, was selected for the investigation of zeolite 5A structure to act as a drug carrier. In a first set of experiments, the zeolite carrier capacity was tested by analyzing the adsorption of curcumin from liquid solutions within the framework of the zeolite. This approach was dependent on the diffusion of the drug in an environment that mediated its exposure to the zeolite framework.

To determine the loading efficiency (LE%), zeolites were incubated with solutions of different curcumin concentration (0.0125, 0.025, 0.05 mol/L in acetone) for 48 h. The maximum concentration of curcumin was selected based on the maximum loading capacity obtained for similar zeolites (2:1 mass ratio of drug to carrier) previously reported in the literature [24]. After the loading was completed, the supernatant solutions with residual drug were separated by sedimentation and analyzed by UV-vis spectroscopy [25, 26]. In the UV-vis spectra (Fig. 3), the presence of residual drug was evidenced by the appearance of an intense band occurring in the same position of the curcumin band in acetone ($\lambda_{\text{max}} = 419 \text{ nm}$). The drug loading efficiency

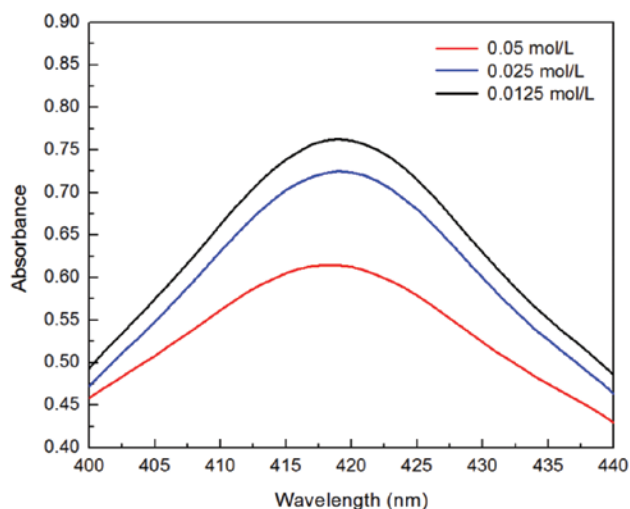


Fig. 3: UV-vis spectra of residual curcumin from incubation solutions with different curcumin concentration (mol/L) after adsorption on zeolite 5A.

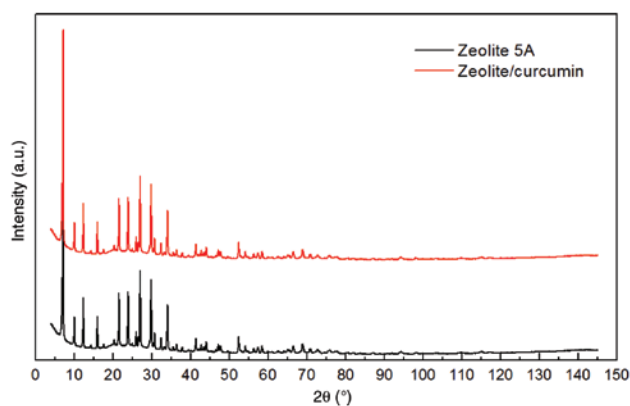


Fig. 4: XRD patterns of empty and curcumin-loaded zeolite 5A (incubation in 0.05 mol/L curcumin solution). The data are offset for clarity.

was determined to be 40 %, 43 % and 51 % for the 0.0125, 0.025 and 0.05 mol/L curcumin incubation solutions, respectively, based on the following formula [27]:

$$LE\% = [(C_0 - C_{sur}) / C_0] \times 100$$

where C_0 is the concentration of curcumin in the initial incubation solution and C_{sur} is the curcumin concentration in the supernatant at the end of the loading procedure. Results from the residual concentration analysis showed that the adsorption of curcumin in the zeolite, and so its loading efficiency, increased upon increasing the initial concentration of curcumin. This effect has been previously observed for other zeolitic frameworks [28], and it is generally explained by the more favorable adsorption of drug molecules on similar molecules that are already immobilized on the zeolite surface. In particular, in our study the maximum loading efficiency for zeolite 5A was obtained when using 0.05 mol/L of curcumin in the incubation solution.

Preservation of the zeolite 5A structure while acting as drug carrier for curcumin was monitored by powder X-ray diffraction (XRD). The XRD patterns of the empty and curcumin-loaded zeolites were recorded at 2θ values between 5° and 140° and they are shown in Fig. 4. A Rietveld refinement analysis was carried to characterize the crystallite size and phase composition (Table 1). From this analysis, the pristine zeolite 5A was determined to be of LTA type with small contaminations by other phases (quartz and calcite) probably formed from the $\text{Ca}(\text{OH})_2$ exchange solution [14]. All investigated curcumin-loaded samples exhibited XRD patterns similar to that of zeolite 5A. No variation was observed in the characteristic zeolite peaks after loading of curcumin, indicating that the framework did not change during the drug loading process. However, the XRD Rietveld refinement data showed a decrease of the crystallite size when increasing the concentration of the loading drug in the zeolite (Table 1). This result is an indication of the encapsulation of curcumin in the zeolite structure, and in particular it can be related to the presence of curcumin in the amorphous and disordered phase of the zeolite [29, 30]. In fact, the nominal pore diameter of the zeolite 5A is 5 Å (according to the manufacturer Zeochem), which is too small to allow for the free diffusion of curcumin inside the sieve

Table 1: XRD Rietveld refinement analysis with calculated crystallite size and phase composition for empty and curcumin-loaded zeolite 5A.

Sample	Zeolite type	a (Å)	Crystallite size (nm)	Microstrain ϵ_0	LTA wt%	Quartz wt%	Calcite wt%
Zeolite 5A	LTA	24.6472(2)	92(2)	0.104(3)	97.41(10)	1.16(5)	1.43(9)
Zeolite/curcumin 0.0125 mol/L	LTA	24.6588(2)	78.2(12)	0.094(3)	96.26(8)	1.60(4)	2.14(7)
Zeolite/curcumin 0.05 mol/L	LTA	24.6586(2)	70.7(10)	0.094(3)	97.30(10)	0.78(5)	1.92(9)

pores. The approximate length of curcumin, as obtained for different conformational isomers by numerical modeling [31], is higher than the average zeolite pore size, suggesting that this drug could have some difficulty in diffusing freely inside the zeolite crystalline structure. Furthermore, the density of the silanol groups on the zeolite surface has a definite impact on the drug loading, since the curcumin molecules interact with surface silanol groups via hydrogen bonding, which promotes curcumin immobilization in the zeolite amorphous and disordered phase. Therefore, there might be a large amount of curcumin on the zeolite 5A surface rather than inside the nanopores, especially for high concentrations of curcumin in the incubation solution (see results by SEM with EDX analysis below). Indeed, the presence of curcumin mainly affects the crystallite size, but not the unit cell of the molecular sieve, as indicated by the Rietveld refinement results in Table 1.

The morphology of the zeolite drug carrier before and after loading of curcumin was studied by SEM analysis (Fig. 5). No significant changes appear in the zeolite morphology and structure after loading of the drug. The SEM images of zeolite 5A and curcumin-loaded zeolite 5A both showed the typical microporous crystalline aluminosilicate structure with no specific change in the average particle diameter of the samples before and after drug loading. Similar results were obtained in previous works on porous drug carriers, such as halloysite-containing microspheres loaded with aspirin and carbonate microparticles loaded with ibuprofen or nifedipine [32, 33].

In addition to the imaging, the energy-dispersive X-ray (EDX) analysis was able to detect the presence of carbon deriving from the organic curcumin molecule on the surface of the drug loaded zeolite samples (Table 2). It is noted that upon increasing the concentration of curcumin in the loading solution the carbon content measured on the zeolite surface increases accordingly. This result confirms that the adsorption of curcumin on zeolite 5A increases with the molecule concentration in the initial incubation solution, as it was determined by UV-vis spectroscopy. Moreover, the ratios of Al, Si and O elements confirmed that there is no substantial variation in the composition of the zeolite 5A before and after curcumin loading.

Evidence for the interaction between the curcumin molecules and the zeolite 5A framework was researched using Fourier-transform infrared (FTIR) spectroscopy. As reported in Fig. 6, for the pure zeolite

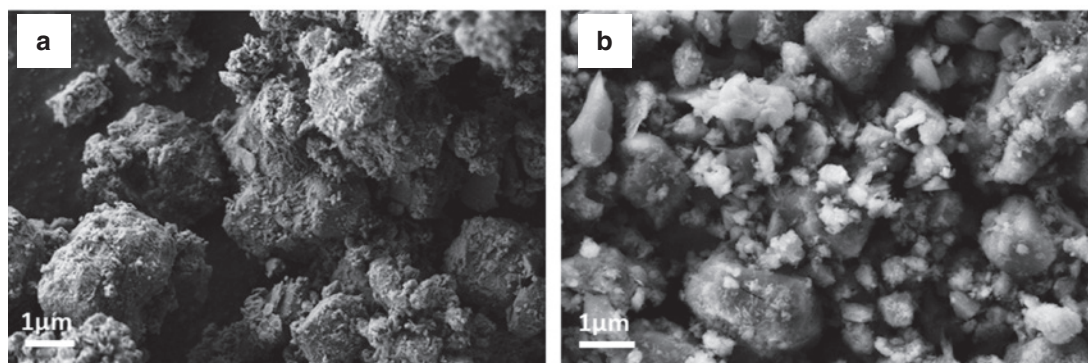


Fig. 5: SEM images of (a) empty zeolite 5A and (b) curcumin-loaded zeolite (incubation in 0.05 mol/L curcumin solution).

Table 2: Energy-dispersive X-ray analysis of empty and curcumin-loaded zeolite 5A (incubation in solutions with different curcumin concentration).

Elements	Zeolite 5A	Zeolite/curcumin 0.0125 mol/L	Zeolite/curcumin 0.025 mol/L	Zeolite/curcumin 0.05 mol/L
O	47.42	49.63	48.53	48.57
Si	27.61	21.25	20.28	19.82
Al	11.61	12.88	13.13	12.63
Ca	6.80	10.04	10.87	10.02
C	1.18	1.66	2.43	4.32

5A sample, characteristic FTIR bands corresponding to the lattice vibrations were observed at wavenumbers from 1700 to 800 cm^{-1} . The broad peak at 1013 cm^{-1} is due to asymmetric stretching vibration of O–Si–O groups, whereas the O–H deformation band appears at 1640 cm^{-1} [34–36]. The FTIR spectrum of curcumin in Figs. 6 and 7 shows characteristic bands at 2917, 2849 and 1427 cm^{-1} , which can be attributed to C–H stretching and to deformation of methyl groups [37–39]. The two peaks at 1627 and 1502 cm^{-1} correspond to C=C, C=O, and C–C stretching vibration of the benzene ring, whereas the olefinic C–H bending vibration appears at 1438 cm^{-1} , and the aromatic C–O stretching vibration at 1274 cm^{-1} . The bands at 1025 cm^{-1} and 963 cm^{-1} can be attributed to C–O stretching and out-of-plane bending of aromatic C–H bonds, respectively [40–42]. For the curcumin-loaded zeolite, the FTIR spectrum shows bands in the regions 3000–2800 cm^{-1} with two specific peaks (2917 and 2849 cm^{-1}) that are found in the pure curcumin spectrum and not in that of zeolite 5A. Therefore, these peaks can be attributed to the presence of drug on the zeolite. The interaction of curcumin with the zeolite surface was evidenced by the characteristic curcumin peaks that shifted from 1506 to 1512 cm^{-1} , from 1438 to 1442 cm^{-1} and from 1274 to 1281 cm^{-1} as a result of intermolecular hydrogen bonding. In addition, the curcumin bands at 2917 and 2849 cm^{-1} became wider in the spectra of the zeolite after loading, which also

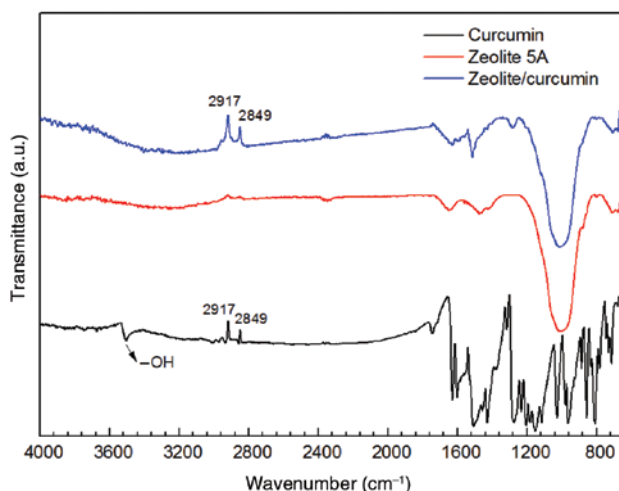


Fig. 6: FTIR spectra of unloaded zeolite 5A, curcumin, and zeolite 5A loaded with curcumin after incubation in 0.05 mol/L solution. The spectra are offset for clarity.

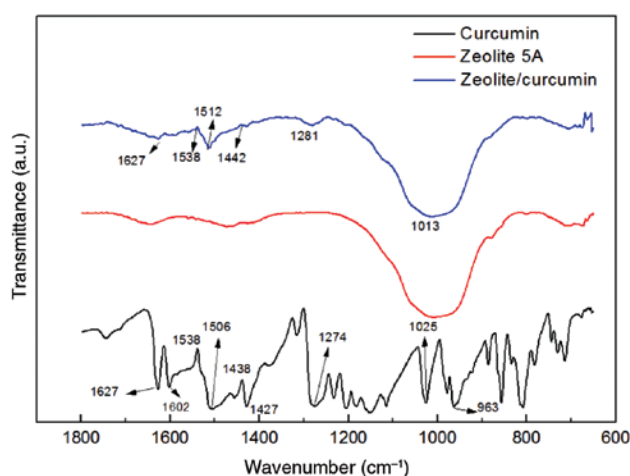


Fig. 7: FTIR spectra of unloaded zeolite 5A, curcumin, and curcumin-loaded zeolite 5A (incubation in 0.05 mol/L curcumin solution) in the fingerprint region.

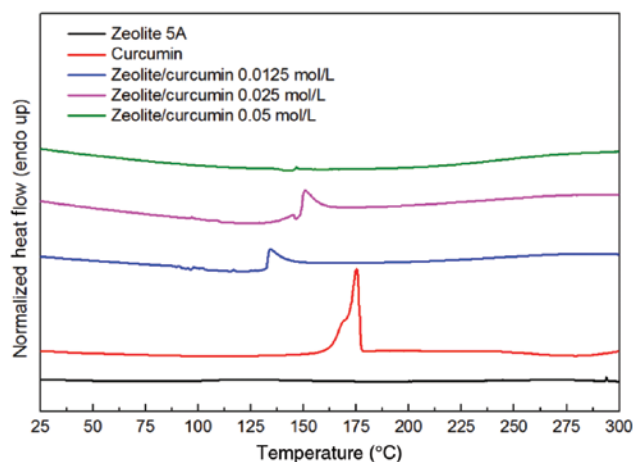


Fig. 8: DSC thermograms of zeolite 5A, curcumin, and curcumin-loaded zeolite 5A after incubation in solutions with different concentrations of curcumin. Heating rate: 10 °C/min. Data are offset for clarity.

suggests an enhancement of the hydrogen bonding. The zeolite vibrational bands, particularly the main band at 1013 cm^{-1} , do not shift or broaden due to curcumin loading, indicating that the zeolite framework remains unchanged after loading, as previously found in studies of drug interaction with similar systems [27, 43].

Investigations by differential scanning calorimetry (DSC) of the empty and curcumin-loaded zeolite 5A samples were performed in the temperature range 25–300 °C. The empty zeolite 5A shows no significant thermal event in the investigated temperature range. On the other hand, the thermograms of pure curcumin powder is characterized by the presence of an endothermic peak at 174 °C due to melting, in agreement with previously reported data [44]. The DSC data of the curcumin-loaded zeolites showed peaks that are shifted with respect to that of pure curcumin, which might be an indication of crystallization of curcumin inside the zeolite pores. According to the literature, the effect of drug crystallizing inside the carrier pores can lead to a melting point occurring at lower temperatures compared to the melting of the drug outside the pores [45, 46]. Indeed, as Fig. 8 shows, there is a shift in the melting point of curcumin, which moves to lower temperatures in the loaded samples. In addition, the shape of the melting peak appears different: melting of free curcumin (outside the pores) is observed as a sharp peak, while drug melting in the pores gives a broader one. This is related to the surface chemistry of the zeolite pores and to the specific interaction of the drug with the pore walls. Results from the DSC analysis complement the XRD Rietveld data indicating a possible change in the crystallinity of curcumin after incorporation in the zeolite framework. In fact, by increasing the curcumin concentration in the initial solution, and so in the zeolite carrier, the interaction of curcumin with the pore walls increases leading to a more disordered state of curcumin, which causes a significant reduction of the melting peak at higher curcumin concentration (0.05 mol/L) with respect to the lower concentration (0.0125 and 0.025 mol/L).

Conclusions

Zeolite 5A, the calcium form of zeolite type A, was used to assess its ability for loading the anticancer drug curcumin. This zeolite structure was selected because of the numerous and accessible pores, making it a favorable candidate for enhanced loading of curcumin. Results from our UV-vis investigation showed that the loading efficiency of curcumin in zeolite 5A is increased by increasing the drug concentration of the initial incubation solution. This observation was confirmed by DSC and XRD analyses, which showed the presence of curcumin inside the zeolite pores and confirmed the stronger interaction of zeolite and curcumin at higher loading concentration. The FTIR analysis was able to detect the presence of curcumin in the zeolite structure

and to determine the hydrogen bonding mechanism as the preferential interaction between curcumin and the zeolite carrier. Both SEM and XRD studies revealed a stable zeolite structure with preservation of its framework integrity after curcumin loading. These results confirmed the presence of curcumin in the zeolite 5A carrier and support the potential use of this porous material as drug carrier in targeted cancer treatments.

Acknowledgements: The authors would like to thank Mauro Ferrini (Department of Chemical Materials and Environmental Engineering, Sapienza University of Rome) for assistance in FTIR spectroscopy. The XRD and FE-SEM analyses were performed at the Center for Nanotechnologies Applied to Engineering (CNIS) of Sapienza University.

References

- [1] H. Kohay, C. Sarisozen, R. Sawant, A. Jhaveri, V. P. Torchilin, Y. G. Mishael. *Acta Biomater.* **55**, 443 (2017).
- [2] Y. M. Lvov, M. M. DeVilliers, R. F. Fakhruddin. *Expert Opin. Drug Deliv.* **13**, 977 (2016).
- [3] P. Figueiredo, K. Lintinen, A. Kiriazis, V. Hynninen, Z. Liu, T. Bauleth-Ramos, A. Rahikkala, A. Correia, T. Kohout, B. Sarmiento, J. Yli-Kauhaluoma, J. Hirvonen, O. Ikkala, M. A. Kostiaainen, H. A. Santos. *Biomaterials* **121**, 97 (2017).
- [4] P. Abasian, M. Radmansouri, M. Habibi Jouybari, M. V. Ghasemi, A. Mohammadi, M. Irani, F. S. Jazi. *Int. J. Biol. Macromol.* **121**, 398 (2019).
- [5] G. Cerri, M. Farina, A. Brundu, A. Daković, P. Giunchedi, E. Gavini, G. Rassa. *Micropor. Mesopor. Mat.* **223**, 58 (2016).
- [6] E. Pérez-Herrero, A. Fernández-Medarde. *Eur. J. Pharm. Biopharm.* **93**, 52 (2015).
- [7] V. Ravinayagam, B. Rabindran Jermy. *J. Saudi Chem. Soc.* (2018).
- [8] P. Tavoraro, S. Catalano, G. Martino, A. Tavoraro. *Appl. Surf. Sci.* **380**, 135 (2016).
- [9] P. Tavoraro, G. Martino, S. Andô, A. Tavoraro. *Mater. Sci. Eng. C* **69**, 894 (2016).
- [10] G. Tegl, V. Stagl, A. Mensah, D. Huber, W. Somitsch, S. Grosse-Kracht, G. M. Guebitz. *Eng. Life Sci.* **18**, 334 (2018).
- [11] B. Sadeghalvad, Z. Ahali, A. Azadmehr. *Arab. J. Sci. Eng.* **41**, 2501 (2016).
- [12] Y.-P. Guo, T. Long, Z.-F. Song, Z.-A. Zhu. *J. Biomed. Mater. Res. B* **102**, 583 (2013).
- [13] E. Khodaverdi, H. A. Soleimani, F. Mohammadpour, F. Hadizadeh. *Chem. Biol. Drug Design* **87**, 849 (2015).
- [14] L. Price, K. Leung, A. Sartbaeva. *Magnetochemistry* **3**, 42 (2017).
- [15] M. Ghadiri, W. Chrzanowski, R. Rohanzadeh. *RSC Adv.* **5**, 29467 (2015).
- [16] C. Karavasili, L. Kokove, I. Kontopoulou, G. K. Eleftheriadis, N. Bouropoulos, D. G. Fatouros. *J. Drug Deliv. Sci. Technol.* **35**, 91 (2016).
- [17] T. Kihara, Y. Zhang, Y. Hu, Q. Mao, Y. Tang, J. Miyake. *J. Biosci. Bioeng.* **111**, 725 (2011).
- [18] C. M. Goodman, C. D. McCusker, T. Yilmaz, V. M. Rotello. *Bioconjug. Chem.* **15**, 897 (2004).
- [19] M. Salem, S. Rohani, E. R. Gillies. *RSC Adv.* **4**, 10815 (2014).
- [20] E. A. M. S. Almeida, I. C. Bellettini, F. P. Garcia, M. T. Farinácio, C. V. Nakamura, A. F. Rubira, A. F. Martins, E. C. Muniz. *Carbohydr. Polym.* **171**, 259 (2017).
- [21] S. Mangalathillam, N. S. Rejinold, A. Nair, V.-K. Lakshmanan, S. V. Nair, R. Jayakumar. *Nanoscale* **4**, 239 (2012).
- [22] S. Gopi, J. Jacob, K. Varma, S. Jude, A. Amalraj, C. A. Arundhathy, R. George, T. R. Sreeraj, C. Divya, A. B. Kunnumakkara, S. J. Stohs. *Phytother. Res.* **31**, 1883 (2017).
- [23] W. Liu, Y. Zhai, X. Heng, F. Y. Che, W. Chen, D. Sun, G. Zhai. *J. Drug Target.* **24**, 694 (2016).
- [24] R. A. Al-Thawabeia, H. A. Hodali. *J. Chem.* **2015**, 9 (2015).
- [25] T. Hickey, D. Kreutzer, D. J. Burgess, F. Moussy. *Biomaterials* **23**, 1649 (2002).
- [26] X. Yao, X. Niu, K. Ma, P. Huang, J. Grothe, S. Kaskel, Y. Zhu. *Small* **13**, 1602225 (2016).
- [27] N. Sanoj Rejinold, M. Muthunayanan, V. V. Divyarani, P. R. Sreerexha, K. P. Chennazhi, S. V. Nair, H. Tamura, R. Jayakumar. *J. Colloid Interface Sci.* **360**, 39 (2011).
- [28] T. Sağır, M. Huysal, Z. Durmus, B. Z. Kurt, M. Senel, S. Isik. *Biomed. Pharmacother.* **77**, 182 (2016).
- [29] K. Jyoti, M. Baunthiyal, A. Singh. *J. Radiat. Res. Appl. Sci.* **9**, 217 (2016).
- [30] F. A. Maulvi, D. H. Lakdawala, A. A. Shaikh, A. R. Desai, H. H. Choksi, R. J. Vaidya, K. M. Ranch, A. R. Koli, B. A. Vyas, D. O. Shah. *J. Control. Release* **226**, 47 (2016).
- [31] T. M. Kolev, E. A. Velcheva, B. A. Stamboliyska, M. Spitteller. *Int. J. Quantum Chem.* **102**, 1069 (2005).
- [32] X. Li, QianYang, J. Ouyang, H. Yang, S. Chang. *Appl. Clay Sci.* **126**, 306 (2016).
- [33] D. Preisig, D. Haid, F. J. O. Varum, R. Bravo, R. Alles, J. Huwyler, M. Puchkov. *Eur. J. Pharm. Biopharm.* **87**, 548 (2014).
- [34] O. Martinho, N. Vilaça, P. J. G. Castro, R. Amorim, A. M. Fonseca, F. Baltazar, R. M. Reis, I. C. Neves. *RSC Adv.* **5**, 28219 (2015).
- [35] V. Mavrodinova, M. Popova, K. Yoncheva, J. Mihály, Á. Szegedi. *J. Colloid Interface Sci.* **458**, 32 (2015).

- [36] X. Wen, F. Yang, Q.-F. Ke, X.-T. Xie, Y.-P. Guo. *J. Mater. Chem. B* **5**, 7866 (2017).
- [37] S. Esfandiarpour-Boroujeni, S. Bagheri-Khoulenjani, H. Mirzadeh, S. Amanpour. *Carbohydr. Polym.* **168**, 14 (2017).
- [38] L. Miloudi, F. Bonnier, D. Bertrand, H. J. Byrne, X. Perse, I. Chourpa, E. Munnier. *Anal. Bioanal. Chem.* **409**, 4593 (2017).
- [39] H. Sandy Budi, H. Lannie, Y. Yanan, M. Anand Kumar, Antaresti, Y. Chengzhong. *Nanotechnology* **27**, 505605 (2016).
- [40] R. Adami, A. Di Capua, E. Reverchon. *Powder Technol.* **305**, 455 (2017).
- [41] F. Sahne, M. Mohammadi, G. D. Najafpour, A. A. Moghadamnia. *Ind. Crops Prod.* **95**, 686 (2017).
- [42] Z. Zhao, M. Xie, Y. Li, A. Chen, G. Li, J. Zhang, H. Hu, X. Wang, S. Li. *Int. J. Nanomedicine* **10**, 3171 (2015).
- [43] R. Amorim, N. Vilaça, O. Martinho, R. M. Reis, M. Sardo, J. Rocha, A. M. Fonseca, F. Baltazar, I. C. Neves. *J. Phys. Chem. C* **116**, 25642 (2012).
- [44] S. S. D. Kumar, M. Surianarayanan, R. Vijayaraghavan, A. B. Mandal, D. R. MacFarlane. *Eur. J. Pharm. Sci.* **51**, 34 (2014).
- [45] V. Makwana, R. Jain, K. Patel, M. Nivsarkar, A. Joshi. *Int. J. Pharm.* **495**, 439 (2015).
- [46] J. Riikonen, E. Mäkilä, J. Salonen, V.-P. Lehto. *Langmuir* **25**, 6137 (2009).